Effective $J=1/2$ insulating state in Ruddlesden-Popper iridates: An LDA+DMFT study

Hongbin Zhang,* Kristjan Haule, and David Vanderbilt
Department of Physics and Astronomy, Rutgers University, Piscataway, USA
(Dated: today)

Using *ab-initio* methods for correlated electrons in solids, we investigate the metal-insulator transition across the Ruddlesden-Popper (RP) series of iridates and explore the robustness of the $J_{\rm eff}=1/2$ state against band effects due to itineracy, tetragonal distortion, octahedral rotation and Coulomb interaction. We predict the effects of epitaxial strain on the optical conductivity, magnetic moments, and $J_{\rm eff}=1/2$ ground-state wave functions in the RP series. To describe the solution of the many-body problem in an intuitive picture, we introduce a concept of energy-dependent atomic states, which strongly resemble the atomic $J_{\rm eff}=1/2$ states but with coefficients that are energy/time-dependent. We demonstrate that the deviation from the ideal $J_{\rm eff}=1/2$ state is negligible at short time scales for both single- and double-layer iridates, while it becomes quite significant for $Sr_3Ir_2O_7$ at long times and low energy. Interestingly, Sr_2IrO_4 is positioned very close to the $SU(2)$ limit, with only $\sim$3% deviation from the ideal $J_{\rm eff}=1/2$ situation.

Metal-insulator transitions are very common in $3d$ transition-metal oxides due to the small bandwidth of the $3d$ orbitals and the poorly screened electron-electron interaction on the $3d$ ions.[1] Due to the larger spatial extent of the $5d$ orbitals, the $5d$ transition-metal oxides are expected to be more itinerant. However, because of strong spin-orbit coupling (SOC), many $5d$ transition-metal oxides show significant electron-electron correlations and even metal-insulator transitions of possible Mott type. One of the most well-studied $5d$ systems at the localization-delocalization boundary is the Ruddlesden-Popper (RP) series of iridates with chemical formula $Sr_{n+1}Ir_nO_{3n+1}$, where n is the number of $SrIrO_3$ perovskite layers sandwiched between extra SrO layers. Experimentally, Sr_2IrO_4 (214) is a Mott-like magnetic insulator with canted in-plane anti-ferromagnetic (AFM) ordering,[2,3] $Sr_3Ir_2O_7$ (327) is a narrow-gap Slater-like AFM insulator with moments aligned along the c-axis,[4,5] while $SrIrO_3$ (113) is a correlated metal.[6] These compounds have attracted tremendous attention recently[7–9] because of the similarity between 214 and the parent compound La_2CuO_4 of the cuprate superconductors: the structures are the same, the low-energy properties can be modeled by a single band Hubbard-type model,[7] and the magnetic spin wave spectrum in Sr_2IrO_4 shows no observable spin-wave gap.[10] This is quite unexpected because the large SOC and IrO_6 octahedral rotations lead to significant Dzyaloshinsky-Moria interaction. On the other hand, a very different spin-wave spectrum with a large magnon gap was found in the double-layer 327 compound.[11]

Kim *et al.*[7] proposed that the strong SOC and the large octahedral crystal-field splitting between the t_{2g} and e_g states produce an effective $J_{\rm eff}=1/2$ state on the Ir^{4+} ion, where the magnetic moment is isotropic and $SU(2)$-invariant. The $J_{\rm eff}=1/2$ states form a Kramers-doublet and contain an equal mixture of d_{xz}, d_{yz} and d_{xy} orbitals in the form $|\psi_{-1/2}\rangle = (|d_{xy}\uparrow\rangle + |d_{yz}\downarrow\rangle + i\,|d_{xz}\downarrow\rangle)/\sqrt{3}$ and $|\psi_{+1/2}\rangle = (-|d_{xy}\downarrow\rangle + |d_{yz}\uparrow\rangle - i\,|d_{xz}\uparrow\rangle)/\sqrt{3}$. This is the ground state of a single ion in a cubic crystal environment, which carries a magnetic moment of $1\,\mu_B$. Experimentally, the Ir ions in 214 have significantly smaller sublattice magnetic moments of the order of $0.5\,\mu_B$,[2] which demonstrates the importance of itineracy in this system. Moreover, the tetragonal distortions in all members of the RP series of iridates are large, leading to a crystal-field splitting $\Lambda \equiv \varepsilon_{xz} - \varepsilon_{xy}$ between d_{xy} and $d_{xz/yz}$ orbitals that breaks the $SU(2)$ invariance of the magnetic moments. Nevertheless, the absence of resonant X-ray magnetic scattering intensity at the L_2 edge suggests that the electronic state in both the single-layer[12] and double-layer[13] members of the RP series are quite close to the $J_{\rm eff}=1/2$ limit.

In this work we have performed dynamical mean field theory (DMFT) calculations[14] in a charge self-consistent implementation on top of density functional theory (DFT), allowing for a realistic treatment of competing crystal-field, spin-orbit, and Coulomb interactions. Our work provides quantitative answers to the questions of how good is the $J_{\rm eff}=1/2$ description in the RP series of iridates, and how large is the deviation from the isotropic $SU(2)$ magnetic response. We show that the answers to these questions have a time-scale or energy-scale dependence, thus resolving some points of controversy in the literature.

Our *ab-initio* DFT+DMFT implementation[15] is based on the WIEN2k package.[16] The impurity model was solved using the continuous-time quantum Monte Carlo method.[17] To minimize the sign problem, a proper choice of the local basis is required. We first chose pseudo-cubic local axes on each Ir atom adapted to the IrO_6 octahedra, and then performed an exact diagonalization of the impurity levels. The calculations were fully self-consistent in the charge density, chemical potential, impurity levels, lattice and impurity Green's functions, hybridizations, and self-energies. The energy range in computing the hybridizations and self-energies spanned a 20 eV window around the Fermi energy (E_F), allowing us to use a set of system-independent local Coulomb interaction param-

eters U and J. This is in contrast to other DMFT calculations on iridates[18,19] where downfolding to Ir $t_{2g}-$orbitals was performed, so that the proper values of U and J depend sensitively on the screening by the bands eliminated from the model. The value of U for our large energy window was estimated for the undistorted 214 with tetragonal structure (P4/mmm) using the method of Ref. 20, which leads to $U \approx 4.5\,\text{eV}$ and $J \approx 0.8\,\text{eV}$. To properly simulate the non-collinear magnetic state in the 214 compound, we chose different local coordinates on each Ir atom, with local quantization axis of spin in the direction of the ordered magnetic moment, and used proper Wigner rotations of spins and orbitals to transform the local self-energy to a common global axis. The DOS and optical conductivities were computed from analytic continuation of the self-energy from the imaginary frequency axis to real frequencies using an auxiliary Green's function and the maximum-entropy method. The DMFT calculations were performed at 50 K, below the AFM transition temperature of the 214 (240 K)[2] and 327 (280 K)[4]. For comparison, we also carried out DFT+U calculations using the full-potential linearized augmented plane wave (FLAPW) method as implemented in the Elk code.[21] Since DFT+U does not include screening effects, the fully screened interaction on Ir is needed, which is here determined to be $U \approx 2.5\,\text{eV}$ by fitting to the DMFT results. VASP was used to relax the structures when epitaxial strain is considered, with atomic forces converged to $10^{-3}\,\text{eV/Å}$ in the GGA approximation.[22]

The resulted DMFT spectral functions are presented in Fig. 1 for the 214, 327, and 113 compounds, with color coding showing the spectral intensity along $\Gamma-X-M-\Gamma$, and the side panels displaying the corresponding orbital-resolved DOS. The dotted lines show an overlay of the band structures from the GGA+U calculations. Within DMFT, the insulating gap in 214 and 327 are approximately 400 and 300 meV, respectively. There is a significant amount of incoherent spectral weight in the gap, which shows up in the DOS, but is hardly noticeable in the spectral-function plot. The unoccupied electronic states are of mainly $J_{\text{eff}} = 1/2$ character. The first valence state at X is also of $J_{\text{eff}} = 1/2$ character, while the first valence state at Γ is of $J_{\text{eff}} = 3/2$ character, hence the occupied states are an equal mixture of $J_{\text{eff}} = 1/2$ and $J_{\text{eff}} = 3/2$ states. In the DMFT calculation, the topmost valence state at X is about 40 meV closer to E_F than the first valence state at the Γ point, in agreement with recent ARPES measurements,[23,24] but in contrast to GGA+U results, where the first valence state is at the Γ point. This is because the filled orbitals (here $J_{\text{eff}} = 3/2$) tend to be repelled from the Fermi level in DMFT. In 327, the $J_{\text{eff}} = 3/2$ tail at Γ is split into two peaks due to its double-layer structure, consistent with experimental results.[25] Finally, the 113 compound is a strongly correlated metal,[6] with very flat bands around E_F. The effective mass of the t_{2g} states is quite large, *e.g.,* the effective mass of the hole pocket around Γ is about nine times that of bare electron.

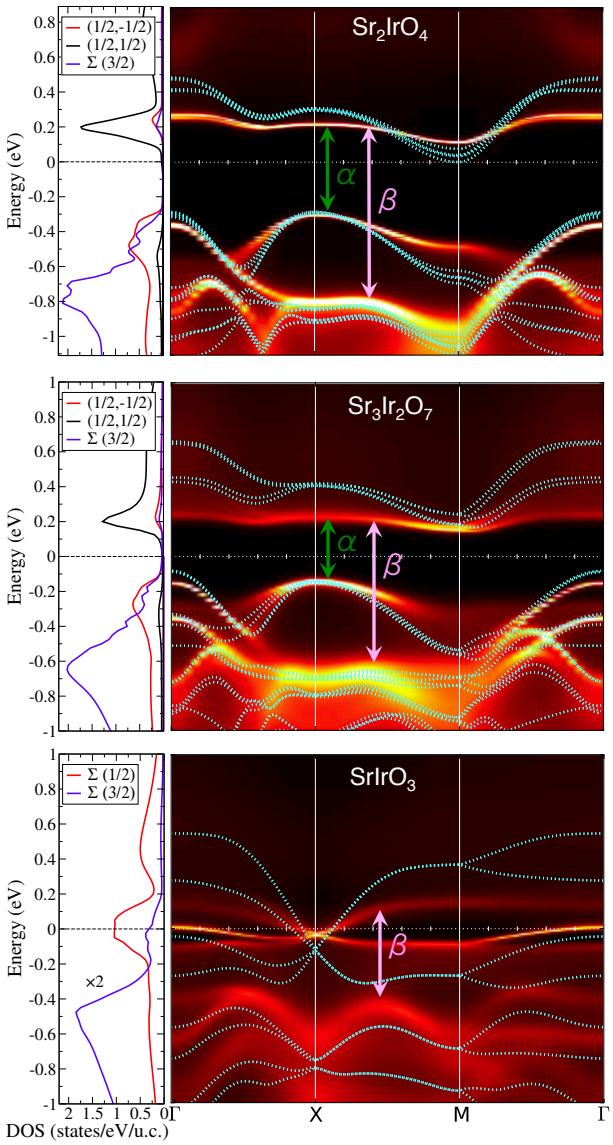

FIG. 1: (Color online) Spectral functions and orbital-resolved densities of states (DOS) obtained by the DMFT method for the RP series of iridates. Arrows indicate optical transitions corresponding to the peaks in the optical conductivities shown in Fig. 2. Dotted lines denote the band structures obtained by GGA+U calculations. For 214 and 327, the GGA+U band structures and the DMFT spectral functions are aligned by fixing the position of the topmost valence state at X. Orbitals $(1/2, \pm 1/2)$ correspond to $\psi_{\pm 1/2}$, and $\sum(3/2)$ stands for the sum over the remaining t_{2g} states, *i.e.*, $J_{\text{eff}} = 3/2$ states.

A closer look at the orbital-resolved DOS in Fig. 1 reveals that the $J_{\text{eff}} = 1/2$ states are not fully polarized. This is due to significant itineracy effects and hybridization between Ir $5d$ and O $2p$ states. The resulting occupation number for the occupied $J_{\text{eff}} = 1/2$ orbitals is about 0.65 (0.45) in the 214 (327) compound. Consequently, this leads to substantially reduced magnetic moments compared to the ideal $J_{\text{eff}} = 1/2$ value of $1\,\mu_B$, down to about $0.55\,\mu_B$ (214) and $0.58\,\mu_B$ (327).

While the most part the GGA+U band structures are in fairly good agreement with the DMFT spectral functions (Fig. 1), there are also some differences. The band gaps in the 214 and 327 compounds within GGA+U are of almost equal size, about 270 meV ($U_{\mathrm{GGA+U}} = 2.5$ eV), while there is a clear gap reduction of about 100 meV in the DMFT calculations. This is not surprising, given that the fully screened U, required by GGA+U, should be reduced in the more itinerant 327 compounds. For 113, the Fermi surface in DMFT is quite similar to the GGA Fermi surface (not shown), but the bandwidth is strongly renormalized. This is not the case in GGA+U, where the hole pocket at Γ is missing. Recent ARPES measurements[26] confirmed the existence of the hole pocket at Γ with a strongly enhanced effective mass, in agreement with the DMFT results.

We mention in passing that the paramagnetic calculation for 214 is not insulating in DFT+DMFT, but a very bad metal, in agreement with the DMFT calculations of Ref. 18, but in disagreement with Ref. 19. The single-site DMFT calculations describe exactly the correlations local to the Ir sites, and also the correlations of infinite range with AFM ordering. Based on magnetic x-ray scattering, Fujiyama *et al.*[3] reported a large but finite correlation length exceeding 100 lattice spacings even 20 K above the Néel temperature in the 214 compound. The "marginal Mott insulator,"[3] a term coined to describe such a short-range ordered state, is not captured by the single site DMFT method, but requires cluster extensions, so unfortunately our modeling cannot account for the properties of this compound near its AFM phase transition.

The optical conductivities for the three compounds obtained by the DMFT calculations are shown in Fig. 2. In agreement with experiments,[27] the optical conductivities of the 214 and 327 insulating compounds have two peaks denoted by α and β in the low-energy range ($0 \sim 1.2$ eV). As proposed in Ref. 28, the α peak is mainly due to the excitations from the highest valence band to the first conduction band, both being primarily of $J_{\mathrm{eff}} = 1/2$ character. The second peak is mainly due to the excitations from the lower valence bands, of primarily $J_{\mathrm{eff}} = 3/2$ character, to the conduction band of $J_{\mathrm{eff}} = 1/2$ character. It is interesting to note that the $J_{\mathrm{eff}} = 1/2$ and $J_{\mathrm{eff}} = 3/2$ valence states strongly overlap in energy, as is clear from the DOS (Fig. 1). Thus, there is no clear separation between the two types of excitations in local quantities, in disagreement with the simple cartoon of Ref. 28. Nevertheless, the vertical excitations probed by optics do give rise to two well separated peaks. Going from 214 to 327, the α peak shifts by about 100 meV to lower energy, while it is replaced by a narrow Drude peak in the 113 compound. The β peak broadens and shifts from 1.0 eV in 214 to 0.5 eV in 113, in good agreement with experiments.[27] We notice that there is an observable tail of optical conductivity in both insulating compounds at low energy (spanning the region from 0.25 eV to about 0.4 eV in 214), which can be attributed to the incoherent

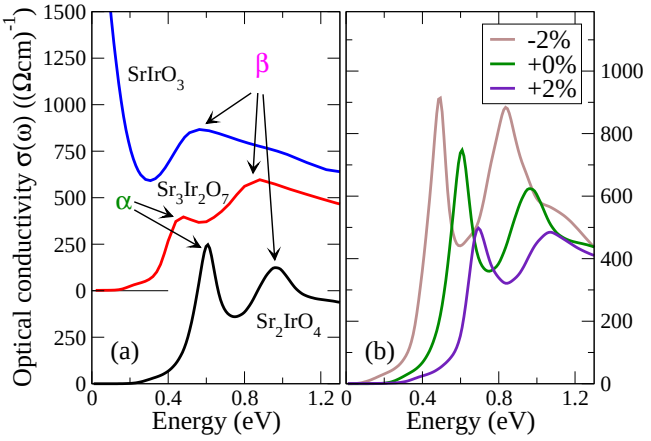

FIG. 2: (Color online) a) Computed optical conductivities σ_1 for three iridates at their experimental lattice constants. For clarity, σ_1 is shifted up by 500 $(\Omega\mathrm{cm})^{-1}$ for $Sr_3Ir_2O_7$ and $SrIrO_3$; α and β indicate peak positions corresponding to the vertical transitions marked in Fig. 1. b) Dependence of σ_1 on epitaxial strain (0% and ±2%) in Sr_2IrO_4.

spectral weight in the gap. A similar tail was also found in optical experiments.[27,28]

To shed more light on the nature of the $J_{\mathrm{eff}} = 1/2$ insulating state, we performed calculations for the RP series of iridates under epitaxial strain, where the out-of-plane lattice parameter and internal lattice coordinates were relaxed in the GGA approximation. Fig. 2(b) shows the optical conductivity for the 214 compound with −2% (compressive), 0%, and +2% (tensile) strain. Compressive (tensile) strain substantially reduces (increases) the gap size due to an increase (decrease) of the dominant in-plane hoppings. The two peaks are shifted to lower (higher) energy, and become sharper (broadened), while the overall conductivity increases (decreases) under compressive (tensile) strain. This is in good agreement with recent optical measurements on strained 214 thin films.[29]

The evolution of the structural parameters under epitaxial strain is shown in Fig. 3. Both the c/a ratio, panels (c) and (f), and the rotation angle θ of the IrO_6 octahedra, panels (b) and (e), decrease nearly linearly with increasing in-plane lattice constants, making the crystal structure less distorted. These structural parameters are in good agreement with recent experiments on thin films.[29]

For the ideal $J_{\mathrm{eff}} = 1/2$ state, which is $SU(2)$ invariant, the orbital magnetic moment on the Ir is twice as large as the spin moment, with values of 2/3 and 1/3 μ_B, respectively. Fig. 3(a) and (d) show the μ_L/μ_S ratio as obtained by the DMFT and GGA+U methods for the 214 and 327 compounds. In 214, this ratio increases with tensile strain, while it decreases in 327. In the absence of strain, $\mu_L/\mu_S \approx 2.2$ for 214 and $\mu_L/\mu_S \approx 1.3$, which demonstrates that the 214 compound has only a slightly larger orbital moment than expected for the ideal $SU(2)$ situation, while 327 has a substantially smaller

orbital moment. For 214 (327) compounds, the $SU(2)$ point can be reached by 1% (3%) compressive strain. It is interesting to note that at this $SU(2)$ point, the IrO_6 octahedra are significantly elongated in the z-direction ($c/a \approx 1.05$). Thus, the deviation from $SU(2)$ behavior is not simply associated with tetragonality, as might have been expected.

To gain some understanding into this puzzling behavior of the magnetic moments, we analyzed the DMFT hybridization function $\Delta(\omega)$, which carries all the information about the crystal environment for an electron on a given iridium site. It is defined by $1/(\omega - \Delta - \Sigma) = \sum_k \hat{P}/(\omega + \mu - \varepsilon_k - \hat{P}^{-1}\Sigma)$. Here Σ is the DMFT self-energy, ε_k are the Kohn-Sham-like eigenvalues, and $\hat{P}$ ($\hat{P}^{-1}$) is the projector (embedder) on the Ir site. In the high-frequency limit, $\Delta(\omega \to \infty) = \sum_k \hat{P}\,(\varepsilon_k - \mu)$ is a matrix whose elements denote the atomic on-site energy levels. It includes both the crystal-field and SOC terms, and is directly related to the so called single-ion anisotropy. The low-energy counterpart $\Delta(\omega = 0)$ is related to the low-energy excitations such as spin waves.

For both 214 and 327 compounds, the hybridization function can be well represented by the matrix

$$\Delta(\omega) = \left(\begin{array}{c|ccc} & xz\uparrow & yz\uparrow & xy\downarrow \\ \hline xz\uparrow & \epsilon & -i\frac{\lambda}{2} & i(\frac{\lambda}{2}+\delta) \\ yz\uparrow & i\frac{\lambda}{2} & \epsilon & -(\frac{\lambda}{2}+\delta) \\ xy\downarrow & -i(\frac{\lambda}{2}+\delta) & -(\frac{\lambda}{2}+\delta) & \epsilon - \Lambda \end{array}\right), \quad (1)$$

where ϵ indicates the on-site energy, λ the SOC strength, Λ the $d_{xz/yz}/d_{xy}$ crystal-field splitting, and δ the renormalization of the SOC between d_{xy} and $d_{xz/yz}$ orbitals. In general, all of these parameters are frequency-dependent. For the above matrix, the largest eigenvalue corresponds to eigenvectors

$$|\psi_{+\frac{1}{2}}\rangle = -\sqrt{\frac{3-2\gamma(\omega)^2}{3}}\,|d_{xy}\downarrow\rangle + \frac{\gamma(\omega)}{\sqrt{3}}(|d_{yz}\uparrow\rangle - i\,|d_{xz}\uparrow\rangle),$$
$$|\psi_{-\frac{1}{2}}\rangle = \sqrt{\frac{3-2\gamma(\omega)^2}{3}}\,|d_{xy}\uparrow\rangle + \frac{\gamma(\omega)}{\sqrt{3}}(|d_{yz}\downarrow\rangle + i\,|d_{xz}\downarrow\rangle). \quad (2)$$

This is a generalization of the ideal $J_{\rm eff} = 1/2$ wave function, which is recovered when $\gamma = 1$. For small deviation from the ideal $SU(2)$ case ($\Lambda/\lambda \ll 1$ and $\delta/\lambda \ll 1$) one finds $\gamma = 1 + \frac{2}{9}\frac{\Lambda-\delta}{\lambda} + \cdots = 1 + \tilde{\gamma}$, where $\tilde{\gamma} \equiv \gamma - 1$ is a small deviation of positive or negative sign for $J_{\rm eff} = 1/2$ states that are respectively expanded or contracted in the z-direction. Within the low-energy subspace of $\psi_{\pm 1/2}$, the orbital and spin moments along z become $\langle \mu_{\rm L}^z \rangle = \frac{2}{3}\gamma^2 \Delta n \approx (\frac{2}{3} + \frac{4}{3}\tilde{\gamma})\Delta n$ and $\langle \mu_{\rm S}^z \rangle = (\frac{4}{3}\gamma^2 - 1)\Delta n \approx (\frac{1}{3} + \frac{8}{3}\tilde{\gamma})\Delta n$, while in-plane they are $\langle \mu_{\rm L}^{xy} \rangle = \frac{2}{3}\gamma\sqrt{3-2\gamma^2}\Delta n \approx (\frac{2}{3} - \frac{2}{3}\tilde{\gamma})\Delta n$ and $\langle \mu_{\rm S}^{xy} \rangle = \frac{3-2\gamma^2}{3}\Delta n \approx (\frac{1}{3} - \frac{4}{3}\tilde{\gamma})\Delta n$, where $\Delta n \equiv n_{1/2} - n_{-1/2}$ is the difference of the occupation numbers of the $\psi_{\pm 1/2}$ states. We checked that the *ab-initio*-obtained values for both orbital and spin moments are well accounted for by these simplified expressions in the low-energy limit, i.e., when $\gamma(\omega = 0)$ is used.

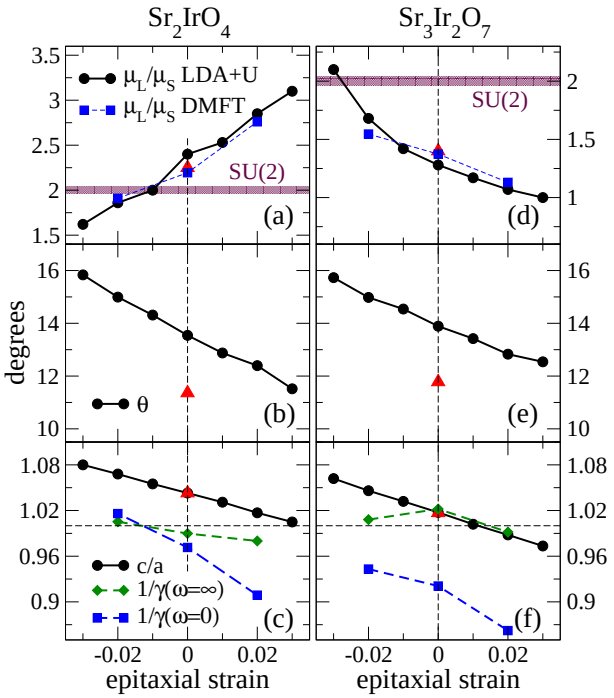

FIG. 3: (colored online) Dependence of computed properties of 214 (a-c) and 327 (d-f) compounds on epitaxial strain in the range of ±3%. (a) and (d): orbital-to-spin moment ratio $\mu_{\rm L}/\mu_{\rm S}$. (b) and (e): staggered rotation angle θ of IrO_6 octahedra. (c) and (f): ratio of Ir-O bond lengths along z and in-plane c/a, and inverse of parameter γ describing the generalized $J_{\rm eff} = 1/2$ wave function (see main text). Filled symbols with dashed (solid black) lines denote the results obtained by DMFT (GGA+U) calculations. Red triangles indicate GGA+U results computed with unrelaxed experimental lattice parameters.

The values of $1/\gamma(\omega = \infty)$ and $1/\gamma(\omega = 0)$, as obtained by exact diagonalization of the hybridization matrix, are plotted in Figs. 3(c) and (f). In a simplified model, where only splitting between d_{xy} and $d_{yz/xz}$ due to the tetragonal distortion of IrO_6 octahedra is considered, $1/\gamma$ is expected to be directly proportional to the c/a ratio and $1/\gamma = 1.0$ when $c/a = 1$. Clearly this is not the case as shown in Figs. 3(c) and (f). In the high-frequency limit, $\gamma(\omega = \infty)$ deviates from the ideal value of unity by less than 2%, which shows that the single-ion anisotropy is small in both compounds. In the low-frequency limit, which is more relevant for spin dynamics, we can approximate $\gamma(\omega = 0) \approx 1.03 + 3.5r$ in the 214 compound, where r denotes the amount of epitaxial strain. In the absence of strain, this is quite close to unity, and reaches the ideal value upon 0.9% compressive strain ($r = -0.009$). The behavior in the 327 compound is quite different, where we might approximate $\gamma(\omega = 0) \approx 1.08 + 2.5r$. A substantial deviation of 8% from the $SU(2)$ value is obtained in the absence of strain, and more than 3%, compressive strain is necessary to recover an isotropic magnetic moment.

Our *ab-initio* values of $\mu_{\rm L}/\mu_{\rm S}$ are well accounted for by this simplified model when $\gamma(\omega=0)$ is used to evaluate the magnetic moments. In the 214 compound the magnetic moments are ordered in-plane, so that $\mu_{\rm L}^{xy}/\mu_{\rm S}^{xy} \approx (\frac{2}{3}-\frac{2}{3}\tilde{\gamma})/(\frac{1}{3}-\frac{4}{3}\tilde{\gamma}) \approx 2+6\tilde{\gamma} \approx 2.2+21r$, which is quite close to the *ab-initio*-calculated line in Fig. 3(a). In the 327 compound, the AFM moments are ordered in the z-direction, hence $\mu_{\rm L}^{z}/\mu_{\rm S}^{z} \approx (\frac{2}{3}+\frac{4}{3}\tilde{\gamma})/(\frac{1}{3}+\frac{8}{3}\tilde{\gamma}) \approx 2-12\tilde{\gamma} \approx 1.04-30r$. Due to the much larger deviation $\tilde{\gamma}$, this approximation is not very accurate, but it nevertheless gives a decreasing moment ratio $\mu_{\rm L}/\mu_{\rm S}$ with tensile strain and a large deviation of this ratio from the ideal $SU(2)$ value of 2. Therefore, we conclude that the low-energy magnetic excitations in 214 are quite close to the ideal $SU(2)$ isotropic case, with only 3% larger $d_{xz/yz}$ contributions to the ground-state wave function than that of its d_{xy} component. On the other hand, in 327 there is substantially more $d_{xz/yz}$ character ($\approx 8\%$) in the low-energy wave function, which leads to larger moments in the z-direction and a smaller $\mu_{\rm L}/\mu_{\rm S}$ ratio.

Finally, let us comment on the *ab-initio* values of the entries in the hybridization matrix, Eq. 1. At high frequency $\Delta(\omega\to\infty)$, the crystal-field splitting is typically only $\Lambda \approx 25$ meV, while the SOC strength $\lambda/2 \approx 250$ meV, and the SOC enhancement δ vanishes. This gives $\gamma(\omega=\infty)\approx 1.01$, as shown in Figs. 3(d) and (h). At low energy, the crystal-field splitting is strongly enhanced by the hybridization effects of the tetragonal crystal structure. In 214, it typically takes a value of $\Lambda \approx 140$ meV. Unexpectedly, δ is of similar magnitude in the 214 compounds, hence $\gamma(\omega=0)\approx 1+\frac{2}{9}(\Lambda-\delta)/\lambda$ is again close to unity. In 327 the enhancement of crystal fields is even larger ($\Lambda \approx 300$ meV), but δ is somewhat smaller ($\delta \approx 120$ meV) compared to that in 214, so that a significant deviation from the ideal value is observed ($\gamma \approx 1.08$). We note that the proximity to the $SU(2)$-invariant point leads to isotropic moments and almost gapless spin wave excitations, which is in qualitative agreement with recent measurements where a small spin gap was found in the 214 compound[10] and a large spin gap in the 327 compound.[11] We also note that fast experimental probes should be more consistent with our $\Delta(\omega\to\infty)$ limit, with a more $SU(2)-$like symmetric response ($\gamma(\omega=\infty)\approx 1$), while low-energy probes should see larger deviations from this limit ($\gamma(\omega=0)$ as in Fig. 3).

Acknowledgments We acknowledge insightful discussions with George Jackeli, Kyle Shen, Jaejun Yu. This work was supported by NSF Grant DMREF-12-33349.

Note added: While this manuscript was in preparation, we became aware of work by Fujiyama *et.al*[31], where the ratio μ_L/μ_S of 214 was estimated to be 2.5 ± 0.35 by NRMXS measurements, close to our theoretical value of $\mu_L/\mu_S \approx 2.2$.

* corresp. author: hzhang@physics.rutgers.edu

1. M. Imada, A. Fujimori, and Y. Tokura, Rev. Mod. Phys. **70**, 1039 (1998).
2. G. Cao, J. Bolivar, S. McCall, J.E. Crow, and R.P. Guertin, Phys. Rev. B **57**, R11039 (1998).
3. S. Fujiyama, H. Ohsumi, T. Komesu, J. Matsuno, B.J. Kim, M. Takata, T. Arima, and H. Takagi, Phys. Rev. Lett. **108**, 247212 (2012).
4. G. Cao, Y. Xin, C.S. Alexander, J.E. Crow, P. Schlottmann, M.K. Crawford, R.L. Harlow, and W. Marshall, Phys. Rev. B **66**, 214412 (2002).
5. S. Fujiyama, K. Ohashi, H. Ohsumi, K. Sugimoto, T. Takayama, T. Komesu, M. Takata, T. Arima, and H. Takagi, Phys. Rev. B **86**, 174414 (2012).
6. G. Cao, V. Duarairaj, S. Chikara, L.E. DeLong, S. Parkin, and P. Schlottmann, Phys. Rev. B **76**, 100420(R) (2007).
7. B.J. Kim, H. Jin, S.J. Moon, J.-Y. Kim, B.-G. Park, C.S. Leem, J. Yu, T.W. Noh, C.Kim, S.-J. Oh, J.-H. Park, V. Durairaj, G. Cao, and E. Rotenberg, Phys. Rev. Lett. **101**, 076402 (2008).
8. G. Jackeli, and G. Khaliullin, Phys. Rev. Lett. **102**, 017205 (2009).
9. F. Wang, and T. Senthil, Phys. Rev. Lett. **106**, 136402 (2011).
10. J. Kim, D. Casa, M.H. Upton, T. Gog, Y.-J. Kim, J.F. Mitchell, M. van Veenendaal, M. Daghofer, J. van den Brink, G. Khaliullin, and B.J. Kim, Phys. Rev. Lett. **108**, 177003 (2012).
11. J. Kim, A.H. Said, D. Casa, M.H. Upton, T. Gog, M. Daghofer, G. Jackeli, J. van den Brink, G. Khaliullin, and B.J. Kim, Phys. Rev. Lett. **109**, 157402 (2012).
12. B.J. Kim, H. Ohsumi, T. Komesu, S. Sakai, T. Morita, H. Takagi, and T. Arima, Science **323**, 1329 (2009).
13. S. Boseggia, R. Springell, H.C. Walker, A.T. Boothroyd, D. Prabhakaran, D. Wermeille, L. Bouchenoire, S.P. Collins, and D.F. McMorrow, Phys. Rev. B **85** 184432 (2012).
14. G. Kotliar, S.Y. Savrasov, K. Haule, V.S. Oudovenko, O. Parcollet, and C.A. Marianetti, Rev. Mod. Phys. **78**, 865 (2006).
15. K. Haule, C.-H. Yee, and K. Kim, Phys. Rev. B **81**, 195107 (2010).
16. http://www.wien2k.at
17. K. Haule, Phys. Rev. B **75**, 155113 (2007).
18. R. Arita, J. Kunes, A.V. Kozhevnikov, A.G. Eguiluz, and M. Imada, Phys. Rev. Lett. **108**, 086403 (2012).
19. C. Martins, M. Aichhorn, L. Vaugier, and S. Biermann, Phys. Rev. Lett. **107**, 266404 (2011).
20. A. Kutepov, K. Haule, S.Y. Savrasov, and G. Kotliar, Phys. Rev. B **82**, 045105 (2010).
21. http://elk.sourceforge.net
22. http://www.vasp.at
23. B.M. Wojek, M.H. Berntsen, S. Boseggia, A.T. Boothroyd, D.F. McMorrow, H.M. Rønnow, J. Chang, and O. Tjernberg, J. Phys.: Condens. Matter **24**, 415602 (2012).
24. Q. Wang, Y. Cao, J.A. Waugh, S.R. Park, T.F. Qi, O.B. Korneta, G. Cao, and D.S. Dessau, Phys. Rev. B **87**, 245109 (2013).
25. P.D.C. King, T. Takayama, A. Tamai, E. Rozbicki, S.M. Walker, M. Shi, L. Patthey, R.G. Moore, D. Lu, K.M. Shen, H. Takagi, and F. Baumberger, Phys. Rev. B **87**,

241106 (2013).
[26] Y. Nie, P.D.C. King, and K.M. Shen, *private communication*
[27] S.J. Moon, H. Jin, K.W. Kim, W. S. Choi, Y.S. Lee, J. Yu, *et al.*, Phys. Rev. Lett. **101**, 226402 (2008).
[28] S.J. Moon, H. Jin, W.S. Choi, J.S. Lee, S.S.A. Seo, J. Yu, G. Cao, T.W. Noh, and Y.S. Lee, Phys. Rev. B **80**, 195110 (2009).
[29] J. Nichols, J. Terzic, E.G. Bittle, O.B. Korneta, L.E. De Long, J.W. Brill, G. Cao, and S.S.A. Seo, arXiv:1302.0918
[30] H. Jin, H. Jeong, T. Ozaki, and J. Yu, Phys. Rev. B **80**, 075112 (2009).
[31] S. Fujiyama, H. Ohsumi, K. Ohashi, D. Hirai, B.J. Kim, T. Arima, M. Takata, H. Takagi, arXiv:1308.0923.